Liquid-Phase Polymerization of Propylene with a Highly Active Catalyst

Job Jan C. Samson, Günter Weickert, Annelies E. Heerze, and K. Roel Westerterp
Chemical Reaction Engineering Laboratories, Dept. of Chemical Engineering, Twente University of Technology,
7500 AE Enschede, The Netherlands

An experimental setup and a kinetic study of the polymerization of propylene in liquid monomer with a highly active catalyst are presented. The purification system for monomer, the catalyst injection system, the temperature control system, and the polymerization procedures are described in detail. Further, reproducibility of the experiments is tested, the kinetics are described in the temperature range of 27 to 67°C, and the influence of prepolymerization in cold liquid propylene is investigated.

Introduction

Despite the importance of the polyolefin processes, relatively few experimental studies are found in the public literature because downscaling of these polymerizations is so difficult. The downscaling problems are caused by the high activity of the catalyst and its sensitivity to small traces of impurities, like H_2O and O_2, making the reproducible introduction of a few mg of catalyst into the reactor difficult. Other problems are the availability of high-activity catalysts for public research and the high costs of experimental research in this field. Moreover, the reactions are strongly exothermic, making accurate control of the reactor temperature very difficult.

At present, almost all kinetic studies of olefin polymerizations are carried out at low pressures in a diluent, such as heptane, although it is known that the nature of the diluent influences the polymerization process and polymer quality and that mass-transfer limitations may play a role (Yuan and Ray, 1982). In polymerizations with either liquid or gaseous monomer the use of a diluent is avoided. Polymerizations in liquid monomer, compared to polymerizations in the gas phase, exhibit much better heat transfer around growing particles, so that thermal runaway in highly active particles is prevented. On the other hand, polymerizations in liquid monomer are difficult because of the higher pressures and the difficulties in measuring the reaction rate in such a system. We have been able to control these problems in a satisfactory way. This article reports on an experimental setup for the polymerization in liquid propylene in which a systematic kinetic study has been performed using a highly active

$MgCl_2$/$TiCl_4$/ethylbenzoate catalyst containing a few percent of titanium (see, for comparison, Kim and Woo (1990)). The catalyst is used in conjunction with triethylaluminum (TEA) as cocatalyst and paraethoxyethylbenzoate (PEEB) as electron donor. The reaction is executed in liquid propylene to study reaction rates and catalyst aging at different temperatures. In addition, the effect of prepolymerization on the reaction rate is investigated.

Experimental Setup

Materials and purification

Table 1 shows the component specifications from the bottle packs we have used. A large amount of one, the same batch of propylene and catalyst components, has been bought to ensure constant quality for a long series of experiments over a long time. Propylene, pentane, hydrogen, and nitrogen

Table 1. Specifications of the Purchased Components

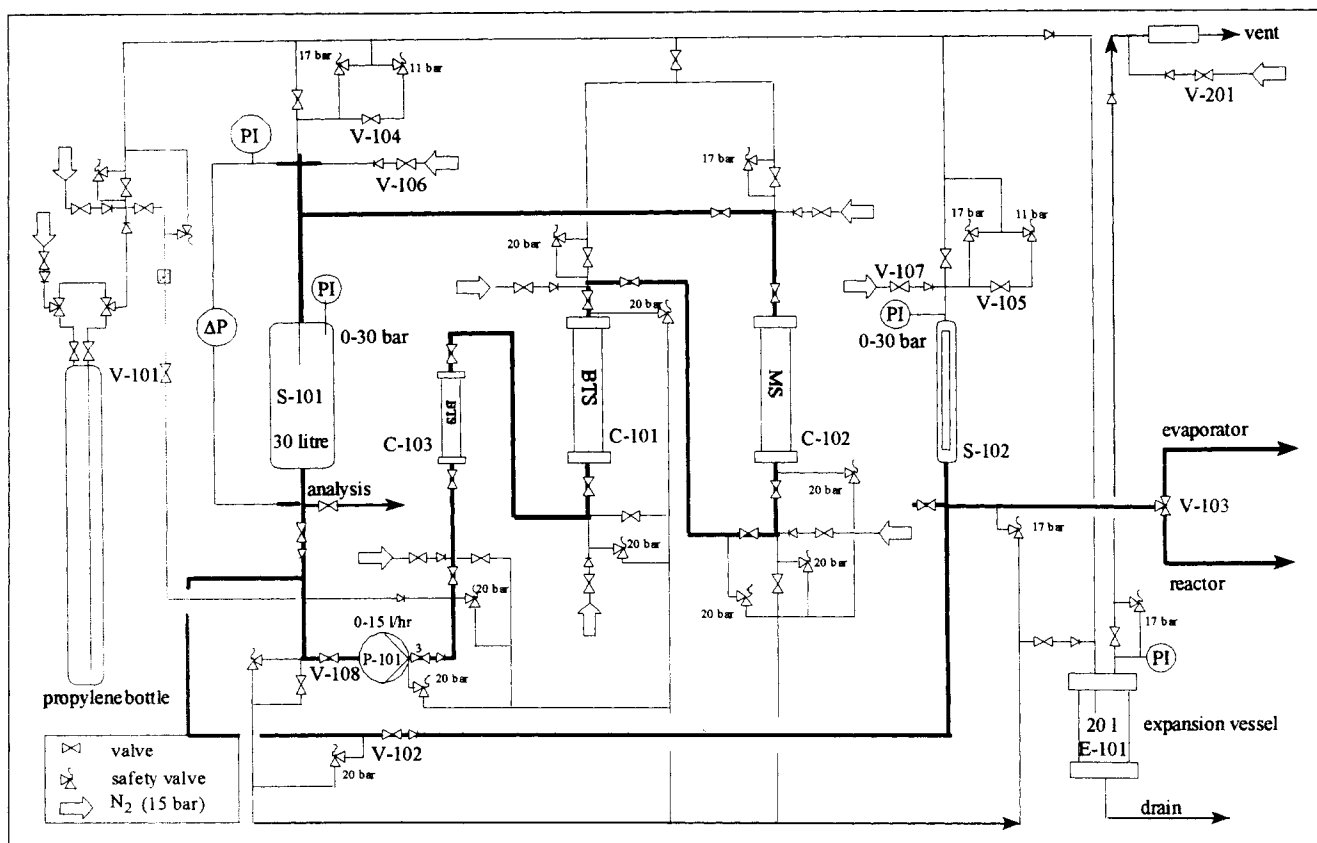| Component	Supplier	Specifications
Propylene	Prax Air	$C_3H_6 > 99.5\%$; $O_2 < 5$ ppm; $H_2O < 1$ ppm; $CO < 0.1$ ppm; $CO_2 < 0.8$ ppm
TEAl	AKZO-NOBEL	$TEAl > 96\%$; $AlH_3 < 0.07\%$
DEAC	AKZO-NOBEL	
Pentane	Merck	$C_5H_{12} > 99.5\%$; pro analysis
H_2	Prax Air	$H_2 > 99.999\%$
N_2	Hoekloos	$N_2 > 99.999\%$
BASF R3-11	BASF	
Molsieves 3A, 4A, 13X	Aldrich	

Figure 1. Purification system for liquid propylene.

are cleaned thoroughly in separate purification systems to remove traces of CO, O_2, H_2O, sulfurous components, and so on. The purification systems are described below.

Monomer Purification. The purification system for liquid propylene is shown in Figure 1. Liquid propylene from the bottle is pressed into a 25-L storage vessel (S-101) by nitrogen overpressure over three purification columns in series. The first column has a volume of one liter and is packed with a bed of oxidized *BASF R3-11* catalyst to oxidize CO to CO_2. The second column has a volume of 17 L and is packed with reduced *BASF R3-11* catalyst to chemisorb oxygen. The third column, also with a volume of 17 L, is packed with successive beds of molecular sieves of types 3A, 4A, and 13X to absorb H_2O, CO_2, and other impurities. For further cleaning after the storage vessel has been filled with propylene from the bottle, the stored propylene is continuously recirculated over the columns using a *Lewa EK-M-510V1* membrane pump. The propylene quality is monitored by measuring the oxygen and water concentrations with an *AMS 3180* oxygen analyzer and a *Fluidsysteme PPB 30* water analyzer, respectively. When the water and oxygen concentrations are below 0.1 ppm, vessel S-102 is filled. S-102 is a 5-L vessel equipped with an electronic, as well as an optical-level, indicator and is used to dose a prescribed amount of propylene in the reactor.

Pentane Purification. Liquid pentane from a 10-L drum is pressed by nitrogen overpressure over two successive purification columns, packed with reduced *BASF R3-11* and molecular sieves of types 3A, 4A, and 13X, respectively, into a 3-L storage vessel. After this storage vessel has been filled,

the contents are continuously recirculated over the columns for further cleaning.

Purification of Gases. Nitrogen and hydrogen of the highest purity are further cleaned by leading the components in the gas phase and at ambient temperature over two columns in series, packed with reduced *BASF R3-11* and molecular sieves of types 3A, 4A, and 13X, respectively.

Catalyst storage and handling

Catalyst, cocatalyst, and electron donor are stored and handled under nitrogen in a *Braun MB 150 B-G-1* glove box. The nitrogen atmosphere contains less than 0.1 ppm H_2O and O_2. For each experiment, the desired amounts of catalyst, cocatalyst, and electron donor are put into separate vials used for injections.

Catalyst injection system

The injection system shown in Figure 2 safeguards inert conditions during injection as well as diluting the catalyst before injection into the reactor. First, the 20-mL vial containing the catalyst component is connected to the injection system by pricking the sharpened capillaries through the septum of the vial. After connection to the injection system, the vial is flushed with a stream of nitrogen that enters by the longer capillary at 0.5 bar and leaves the vial by the safety valve of the shorter capillary. In the next step, about 10 mL of pentane is added to the vial to dilute and suspend the
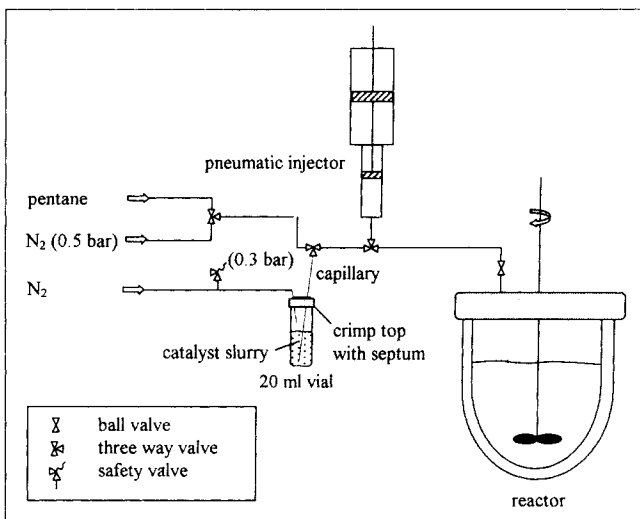
Figure 2. Catalyst injection system.

catalyst. While shaking the vial intensively (Perry, 1973), the catalyst suspension is quickly sucked into the intermediate chamber of the injector and quickly injected into the reactor. After injection of the catalyst, the injection procedure is repeated three times using a fresh portion of pentane to flush the vial, piping, and injector in order to minimize catalyst losses.

Reactor system

The reactor system (Figure 3) comprises a *Büchi BEP 280* stirred laboratory autoclave system for pressures up to 40 bar. The 5-L reactor vessel is equipped with a heating jacket and a separately heated cover plate. An explosionproof motor, with a variable speed transmission of up to 2,000 rpm, drives the magnetically coupled stirrer. A turbine stirrer is attached to a specially designed hollow shaft, which disperses gas from
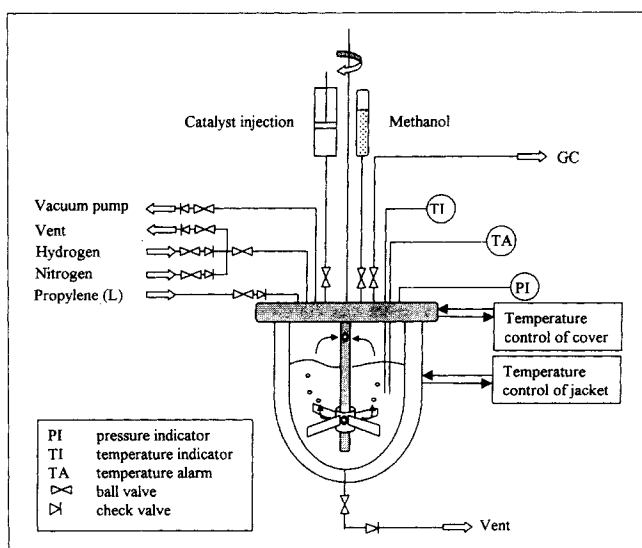
the gas cap into the liquid. An electronic pressure gauge and thermocouples are used to measure reactor pressure and temperatures, respectively.

Temperature control system

Figure 4 shows the temperature control, which comprises separate control circuits for the reactor cover plate and the reactor jacket. The temperature of the cover plate is always set a few degrees above the reaction temperature. The control circuit of the reactor jacket comprises cold- and hot-water streams, a pipe that injects cold water directly into the inlet pipe of the reactor jacket, and an Eurotherm 900 EPC proportional-integral-derivative (PID) control unit. The separate hot- and cold-water streams are required to heat a cold reactor in a few minutes from prepolymerization conditions to higher reaction temperatures. The temperature control system is fast and accurate, with a maximum overshoot of 0.5 to 1.0°C in the first minutes of the reaction. After that, the reactor temperature is maintained constant within 0.1°C.

Reaction-rate measurements

Concentration Measurements by GC. The reaction rate has been determined in different ways. At first, we measured the concentration of an inert tracer, propane, in the gas phase of the reactor by GC every 3 min, and calculated the propylene consumption in that time interval with the following equation:

$$R_p = \frac{N_{t_0} - N_{t_1}}{m_c * (t_1 - t_0)}, \tag{1}$$

where m_c is the mass of the $MgCl_2/TiCl_4/EB$ catalyst particles injected into the reactor, and N_{t_0} and N_{t_1} are the number of moles of propylene in the reactor at times t_0 and t_1, respectively. The initial amounts of propylene and propane are calculated from the initial amount of composition of the liquid added to the reactor. At time t_0, the following balance holds for the total amount of propylene in the reactor:
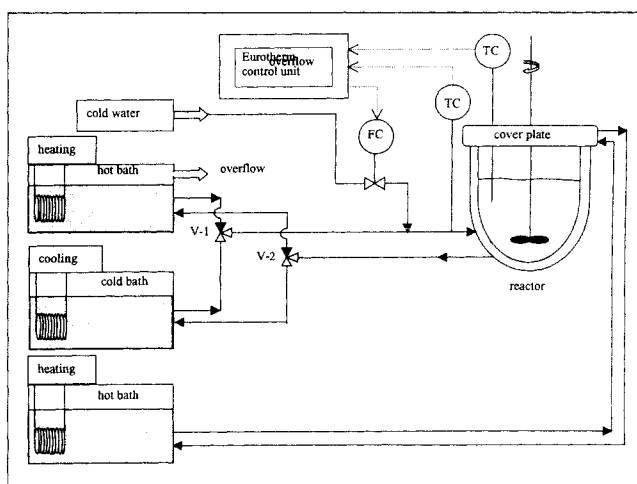

Figure 3. Reactor system for liquid monomer polymerizations.

Figure 4. Reactor temperature control system for reactions with and without prepolymerization.

$$N_{t_0} = (1-x)N_{L,\text{tot},t_0} + (1-y)N_{G,\text{tot},t_0}, \qquad (2)$$

where x and y are the molar fractions of propane in the liquid and gas phases, respectively, and N_{L,tot,t_0} and N_{G,tot,t_0} are the total number of moles in the liquid and gas phase, respectively.

At time t_1, the total number of moles of propylene in the reactor is calculated using the fraction of propane measured at t_1:

$$N_{t_1} = (1-x)N_{L,\text{tot},t_1} + (1-y)N_{G,\text{tot},t_1}. \qquad (3)$$

The number of moles at t_1 in the liquid and the gas phases is calculated with an iterative procedure using the number of moles in the liquid and gas phases at t_0 as starting values. The molar fraction of propane in the gas cap is measured by GC; further composition of the liquid and gas phases is calculated with the Peng–Robinson equation of state, assuming liquid–vapor equilibrium. With the calculated number of moles in the liquid and gas phase at time t_1, the reaction rate in the time interval from t_0 to t_1 is calculated with Eq. 1. The yield in this time interval is expressed by the following equation:

$$Y = R_p * (t_1 - t_0). \qquad (4)$$

The reaction-rate curve and the overall yield are obtained by calculating the reaction rate and yield over all the time intervals between two sequential GC measurements. As an overall check of the mass balance, the calculated yield is compared to the weighed yield of the polymerization experiment.

Calorimetric Measurements. To determine the reaction rate as a function of time, we also have used a calorimetric method. This method is based on the heat balance of the reactor, given by the following equation:

$$C_{p,r}\frac{dT_r}{dt} = (h_L \cdot A_L + h_G \cdot A_G)\cdot(T_j - T_r)$$
$$+ Q_{\text{cover plate}} + Q_{\text{stirrer}} + m_c \cdot R_p \cdot \Delta H_r, \quad (5)$$

where h_L and h_G are the heat-transfer coefficients of the wetted and nonwetted parts of the inner wall of the reactor to the jacket, respectively; A_L and A_G are the wetted and nonwetted areas of the reactor inner wall, respectively; T_j is the temperature of the reactor jacket estimated by averaging the temperature of the water at the in- and outlet of the reactor jacket:

$$T_j = \frac{T_{j,\text{inlet}} + T_{j,\text{outlet}}}{2}. \qquad (6)$$

At isothermal conditions the accumulation of heat in the reactor, represented by the term at the left side of Eq. 5, is zero. The first two terms on the right side represent the heat transfer through the wetted and the nonwetted inner wall of the reactor, respectively. The third term represents the heat input through the nonwetted cover plate and is negligible, as the temperature of the cover plate is maintained only a few degrees above the reactor temperature. The fourth term rep-

resents the input of energy by the stirrer and is estimated at 7 W, which we have neglected compared to the last term of this equation representing the heat of polymerization.

At isothermal reaction conditions and when neglecting the heat input via the cover plate and the stirrer, Eq. 5 can be simplified. A further simplification is obtained when the heat transfer through the reactor wall is calculated by using an average heat-transfer coefficient. This seems a reasonable assumption because the wetted area of the reactor wall does not change too much as long as conversions are kept relatively low, say, below about 40%. Taking the simplifications just mentioned into account, Eq. 5 can be rearranged into the following equation, expressing the reaction rate as a function of the temperature difference between the reactor and reactor jacket:

$$R_p \approx \frac{\bar{h}\cdot(A_r - A_{\text{cover plate}})\cdot(T_r - T_j)}{m_c\cdot\Delta H_r} \qquad (7)$$

where $\bar{h}$ is the average heat transfer coefficient, A_r the area of the reactor wall, and m_c the mass of $MgCl_2/TiCl_4/EB$ catalyst. The value of $\bar{h}$ has been estimated to be 450 W/m^{2}K. Figure 5 shows that the reaction-rate curves almost coincide if calculated with and without taking the variable wetted area of the reactor inner wall into account. Thus, the error made by using an average heat-transfer coefficient is very small.

The average heat-transfer coefficient has been assumed to be constant during the course of the reaction. In our reaction system, this assumption is only acceptable for propylene conversions below 40 to 50%, depending on the stirrer type and speed. Above conversions of about 40 to 50%, we observe a sharp transition point where the temperature difference between the reactor and the jacket has to be increased significantly to maintain the reactor temperature constant. At the same time the reactor pressure decreases two to three bars. Figure 6 shows the temperatures of the reactor coolant as well as the reactor pressure as a function of time for an experiment in which the transition occurs. After about 60 min the temperature of the reactor rises from 47°C to 47.5°C, and along with that, the pressure increases 0.15 bar. To return the temperature to the reactor setpoint, the coolant temperature has to be decreased permanently by four to eight de-
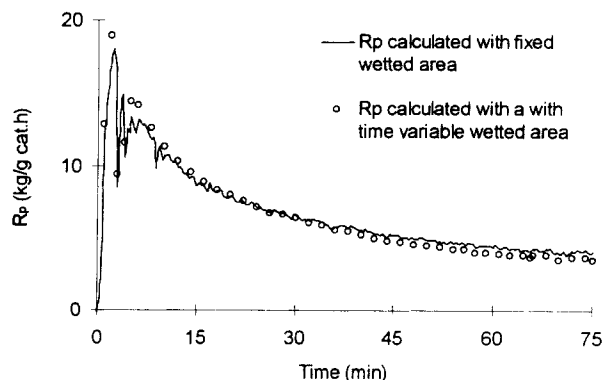

Figure 5. Reaction rate of an experiment, calculated with and without a time-varying wetted area (A_L) of the inner reactor wall.
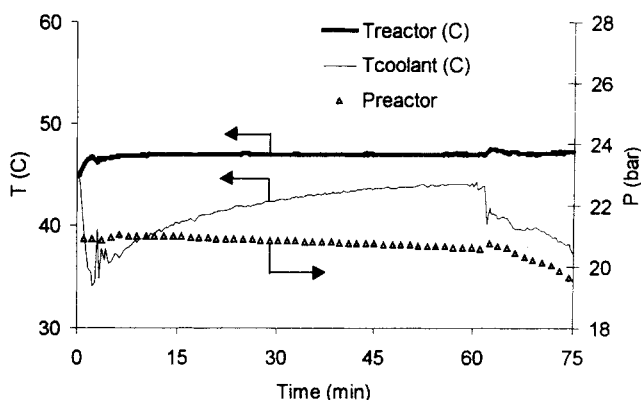
Figure 6. Reactor pressure and temperatures of the reactor and coolant as a function of time in an experiment with a conversion *above* 45%.

grees. Note that the reactor pressure decreases as the coolant temperature decreases and closely follows the course of the coolant temperature. The observed transition in heat-exchange characteristics is ascribed to a change in the hydrodynamic behavior of the propylene/polypropylene slurry in the reactor, which results in insufficient mixing to keep the reactor contents at a constant temperature. At the reactor wall the temperature will decrease below the average reactor temperature, while in the bulk of the slurry the temperature will rise above it. Because the thermocouple is located in the bulk of the slurry at a few centimeters from the reactor wall, the measured temperature is no longer representative of the reactor temperature, but after the transition point it will be higher than the average reactor temperature. The temperature curves of the reactor and coolant as a function of time, shown in Figure 6, do not indicate that such a change occurs before the transition point is reached. In our later experiments the conversions were always kept below 45%.

Prepolymerization

Prepolymerization is a precisely controlled process preceding the polymerization process itself and important for several reasons. First, it prevents a thermal runaway of the highly active primary catalyst particles, which may result in an overly rapid deactivation of the catalyst, poor polymer properties, and poor particle morphology. A thermal runaway as a result of external heat-transfer limitations and its prevention by prepolymerization can be understood from the heat balance over the reacting particle. For the heat transfer from a spherical particle to the bulk surrounding the particle holds:

$$Q = h \cdot A_p \cdot (T_p - T_b). \qquad (8)$$

The heat transfer coefficient (h) is calculated from the Nusselt number:

$$Nu = \frac{h \cdot d_p}{\lambda}, \qquad (9)$$

where Nu is a function of the Reynolds (Re) and the Prandtl number (Pr), see, for example, the following correlation for

heat transfer (Gunn, 1978):

$$Nu = 2 + 1.4 \cdot Re^{0.2} Pr^{0.33} + 0.13 \cdot Re^{0.7} \cdot Pr^{0.33}, \qquad (10)$$

with

$$Re = \left(\frac{\rho \cdot u}{\eta}\right)_{bulk} \cdot d_p \quad \text{and} \quad Pr = \left(\frac{\eta \cdot C_p}{\lambda}\right)_{bulk},$$

where u is the velocity of the free-falling particle in the bulk. Combining Eqs. 8 and 9 gives Eq. 11:

$$Q = Nu \cdot \lambda \cdot \pi \cdot d_p \cdot (T_p - T_b). \qquad (11)$$

Equation 11 shows that the heat-transfer capacity from a catalyst particle to the surrounding bulk increases with increasing particle size. In the early stage of the reaction the primary catalyst particles are at their smallest size, and at the same time at their highest activity. A shortage of external surface area to remove the heat produced by reaction may result in a thermal runaway of the particle, that is, strong overheating compared to the temperature of the surrounding bulk. By slowly increasing the particle size at mild process conditions, sufficient surface area is created to be able to remove all the heat produced in the later stages.

Second, prepolymerization allows the primary catalyst particles to disintegrate into fragments in a controlled way, such that the original particle size is retained. A too-fast growth rate of the primary particles may lead to a sudden breakup into undesired fines.

Third, the prepolymerization gives the associated catalyst components time to diffuse into the core of the primary catalyst particles, to form active centers at all potentially active sites. If the reaction rate were too high in the first seconds of the reaction, a polymer shell might encapsulate the catalyst before it has been completely activated by the cocatalyst. The diffusion rate of propylene through the polymer shell is not limiting, but the diffusion of the much larger molecules of the aluminum alkyl cocatalyst definitely may be. In the case where a polymer shell encapsulates the catalyst particles before the activation process is completed, the final degree of activation of the potential active sites will depend on the nature of the fragmentation process and on the structure of the polymer.

Polymerization Procedures

Polymerization procedure with GC measurements

Before each reaction, the reactor is flushed with nitrogen followed by evacuation for 30 min. Then the reactor is extensively washed with one liter of liquid propylene and 300 mg diethylaluminumchloride (DEAC) at 50°C for one hour to scavenge remaining impurities from the wall and the interior. In the next step, the liquid propylene/DEAC solution is purged through the reactor drain and the remaining gas is vented. Then the reactor is successively filled with a prescribed amount of H_2 and 2.6 L of liquid propylene. While stirring at 1,500 rpm, the reactor is heated to the required reaction temperature. Next, the initial concentration of the tracer component propane, present as an impurity in the

propylene at a level of about 2,000 ppm, is measured. After that TEAl and PEEB are injected successively into the reactor at intervals of one minute. One minute later, the reaction is started by injecting the catalyst. All through the reaction period a sample is taken with the GC equipment every 3 min to determine the propane concentration. The reaction rate is calculated from the mass balance, as derived from the concentration of propane as a function of time. After 75 min of reaction, the polymerization is stopped by adding methanol. Then the unreacted propylene is gently evaporated and the polymer product is removed from the reactor and dried at 50°C in a vacuum oven.

Calorimetric polymerization procedure

The reactor temperatures and the coolant at the inlet and the outlet of the reactor jacket are measured every 20 s and translated into reaction rates by Eq. 7. The method based on the temperature difference between the reactor and the jacket is simpler and generates eight times more measured data points; it further warrants a more stable hydrogen concentration, as there is no need to draw samples from the gas cap during the reaction.

Polymerization procedure with prepolymerization

The reaction is started at a temperature below the required reaction temperature. During this prepolymerization period of typically 1 to 10 min, the reactor temperature is maintained below the required reaction temperature by strong cooling. After the prescribed period of prepolymerization, the temperature of the reactor is rapidly increased to the required reaction temperature. In the heating period itself, it is impossible to estimate the reaction rate, as the reactor is nonisothermal during this period. The reaction rates are calculated for the remaining reaction time; it is also valuable to use them to investigate the influence of prepolymerization on the reaction-rate curve, as is the weighted yield at the end of a reaction.

Kinetics

Kinetic model

In the literature, many models have been proposed to describe the extremely complex reaction kinetics of the polymerization of propylene with Ziegler–Natta catalysts. The kinetics are so complex for different reasons. In the first place, $MgCl_2/TiCl_4$ catalysts produce polymers with a rather broad molecular-weight distribution because of the presence of multiple sites in these catalysts, each site type having its own propagation rate constant and chain transfer rate constant (Böhm, 1978). However, measurement of the individual reaction rates on the various types of sites is impossible. In the second place, Ziegler–Natta catalysts strongly decay with time during polymerization. Many studies have shown that this decay is the result of the decreasing number of active centers over time due to chemical deactivation, rather than a diffusion limitation through the polymer shell encapsulating the catalyst (Doi et al., 1982). Third, the formation of the active centers by complexation of the catalyst with the cocatalyst and the internal and external electron donors is very complex and still not clarified (see Kim and Woo, 1990; Kim et al.,

1991, 1994). Some of the models use the isothermal adsorption isotherms of Langmuir–Hinshelwood, assuming the competitive adsorption reaction of monomer and cocatalyst with the active centers (Tait et al., 1972; Kim et al., 1994). Others describe the catalytic process by the Eley-Rideal mechanism, assuming the complexation of the active Ti-center as the determining step (Böhm, 1978). However, for most catalyst systems the values of the adsorption constants are not available.

To formulate a model to describe the complex kinetics, we have made the following assumptions. First, the propagation rates of the various sites are lumped into a single propagation rate. Second, the catalyst decay through different chemical mechanisms at the various site types is lumped into a single deactivation rate. Third, we use an overall description of the kinetics, presented by the following equation (Zakharov et al., 1983):

$$R_p = k_p C_m C^*, \tag{12}$$

with

$$k_p = k_{p,0} \cdot e^{(E_{a,p}/RT)},$$

where k_p is the propagation rate constant; $E_{a,p}$ is the activation energy for the lumped propagation reactions; T is the temperature; C_m is the concentration of monomer sorbed in the polymer; and C^* is the number of active centers. In many studies, it is confirmed that the reaction rate follows a first-order dependence with respect to the monomer concentration.

The decay of the catalyst is described by a decreasing number of active centers with time, according to the following mathematical equation that has only an empirical meaning:

$$-\frac{dC^*}{dt} = k_d(C^*)^n, \tag{13}$$

with

$$k_d = k_{d,0} \cdot e^{(-E_{a,d}/RT)},$$

where k_d is the deactivation constant; n is the order of deactivation; $E_{a,d}$ is the activation energy for the lumped deactivation reactions; and T is the temperature. Combining Eqs. 12 and 13 gives:

$$-\frac{dR_p}{dt} = K_D \cdot (C_m)^{1-n} \cdot (R_p)^n, \tag{14}$$

with

$$K_D = \frac{k_d}{k_p^{n-1}}.$$

Integration of Eq. 14 gives the reaction rate as a function of time:

$$R_p = \left\{ R_{p,0}^{(1-n)} + (n-1) \cdot K_D \cdot (C_m)^{1-n} \cdot t \right\}^{(1/(1-n))}$$

$$\text{for } n > 1. \quad (15)$$

$$R_p = R_{p,0} \cdot e^{-k_d \cdot t} \qquad \text{for } n = 1, \quad (16)$$

with

$$R_{p,0} = k_p \cdot C_0^* \cdot C_m.$$

Finally, the yield as a function of time is calculated by integrating the reaction rate:

$$Y = \int_0^t R_p \, dt \tag{17}$$

$$Y = \frac{R_{p,0}}{k_d} \left(1 - \exp(-k_d t) \right) \qquad \text{for } n = 1 \quad (18)$$

$$Y = \frac{C_m}{K_D} \cdot \ln \left(1 + R_{p,0} \cdot \frac{K_D}{C_m} \cdot t \right) \qquad \text{for } n = 2 \quad (19)$$

$$Y = \frac{\left[R_{p,0}^{1-n} + (n-1) K_D C_m^{1-n} t \right]^{(2-n)/(1-n)} - R_{p,0}^{2-n}}{(2-n) K_D C_m^{1-n}}$$

$$\text{for } n > 2. \quad (19a)$$

Sorption

Monomer sorption represents the penetration and dispersion of the monomer in the polymer matrix and is directly related to the actual monomer concentration C_m in the polymer, required in Eq. 15. Therefore, knowledge of the sorption behavior as a function of process conditions is crucial for the correct estimate of C_m. A wrong estimate of C_m results in differences in reaction kinetics for slurry, liquid phase, and gas-phase polymerizations, although the mechanism is independent of the reaction phase. It has been shown (Hutchinson and Ray, 1990) that kinetics measured in the (heptane) slurry and the gas phase can be brought together by calculating C_m on the basis of polymer solution thermodynamics. The Flory–Huggins sorption isotherm (see Eq. 20) describes the type of sorption where the interactions between the permeant molecules are relatively strong compared to the permeant/polymer interactions:

$$\ln \frac{P}{P^0} = \ln \phi + (1 - \phi) + \chi (1 - \phi)^2, \tag{20}$$

where P and P^0 are the partial pressure and the saturation vapor pressure of the monomer, respectively; χ is the Flory–Huggins interaction parameter; and ϕ is the volume fraction of permeant sorbed in the amorphous parts of the polymer:
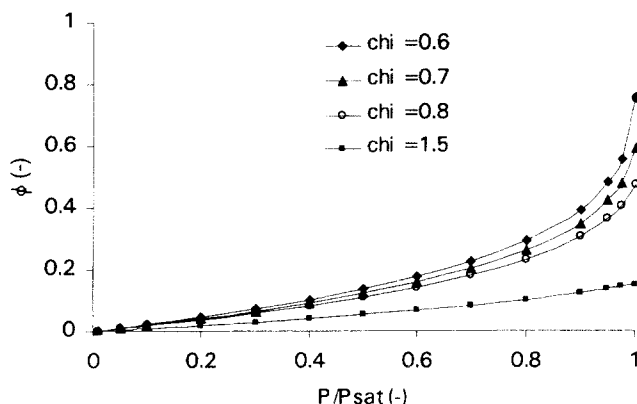
$$\phi = \frac{V_m}{V_m + V_{PP}}, \tag{21}$$

Figure 7. Monomer fraction ϕ in the polymer as a function of the activity (P/P^0) for different values of χ.

where V_m and V_{PP} are the volume fraction of monomer and amorphous polymer in the amorphous polymer/monomer mixture, respectively.

Isotactic polypropylene is a crystalline polymer in which the crystallites keep the amorphous parts together. We assume that the polymer formed *in situ* around the active sites is amorphous before it starts to crystallize partially. Therefore, the monomer concentration in the amorphous polymer, C_m, is the concentration required in the kinetic expression. This concentration was estimated by

$$C_m = \phi \cdot C_L. \tag{22}$$

where C_L is the concentration of liquid monomer surrounding the polymer particle. In Figure 7, the monomer fraction ϕ is given as a function of the activity (P/P^0) for different values of χ. This figure shows that for lower χ-values and activities above 0.5, sorption is enhanced increasingly with increasing pressure. In Figure 8, ϕ is shown as a function of χ at the saturation pressure, that is, at $P/P^0 = 1$, which corresponds to liquid pool conditions. This figure shows that the Flory–Huggins model predicts a polymer and that a perme-
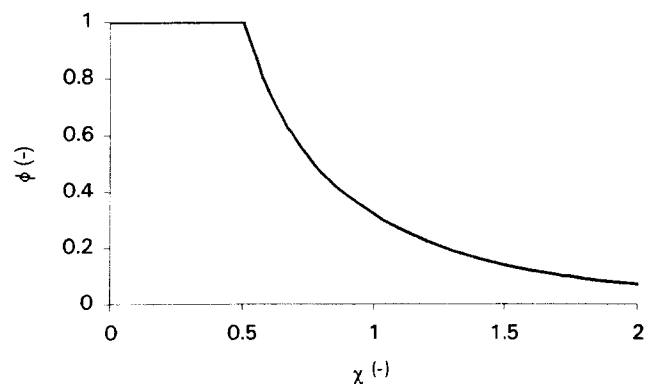

Figure 8. Monomer fraction ϕ in the polymer as a function of the Flory–Huggins interaction parameter at liquid pool conditions, that is, at saturation pressure $(P/P^0 = 1)$.

ant is miscible ($\phi = 1$) over the entire pressure range when χ is below 0.5; for χ-values above 0.5, the polymer is swollen with liquid. Real systems often do not conform to the Flory–Huggins model, but with experimentally determined χ-values this model can predict the sorption behavior rather well. Barton (Barton, 1990) has listed a number of χ-values for different liquids, but liquid propylene is not included. These experimental χ-values vary rather widely, from 0.1 to 2.0, and therefore do not offer a basis for a reliable estimate of the interaction parameter for a propylene/polypropylene system. Therefore, the Flory–Huggins interaction parameter χ has been estimated with the Laar–Hildebrand equation (Barton, 1990):

$$\chi = \left(\frac{v_m}{RT} \right) \cdot (\delta_m - \delta_P)^2 + \beta, \qquad (23)$$

where v_m is the molar volume of the monomer; δ_m and δ_P are the solubility parameters of the monomer and polymer, respectively; and β is the lattice constant, with a value of 0.34 (Aminabhavi et al., 1996). The solubility parameters are calculated from the following correlations (Bradford and Thodos, 1966; Hutchinson and Ray, 1990):

$$\delta_p = 7.7 - 0.0121 \cdot (T - 303.15) \qquad (24)$$

$$\delta_m = \delta_c + k \cdot (1 - T_r)^m, \qquad (25)$$

where δ_c is the solubility parameter at the critical point; T_R the reduced temperature (T/T_c); and k and m are constants. Values for δ_c, k, and m have been tabulated (Bradford and Thodos, 1966) for a number of hydrocarbons; for propylene $\delta_c = 5.077$ (J/cm^3)$^{0.5}$, $k = 15.648$ (J/cm^3)$^{0.5}$, and $m = 0.447$.

Table 2 shows that the calculated values of χ as well as ϕ vary strongly with the temperature: with increasing temperature χ increases from 0.76 to 1.26 and ϕ decreases from 0.5 to 0.2. The values presented in Table 2 have been used in our later calculations.

Results

Comparison of different methods to determine the reaction rate

The two methods we have used to determine the reaction rate as a function of time are compared in Figure 9 for a specific case. Although the reaction rate curve on the basis of the GC measurements follows the typical decay behavior of Ziegler–Natta catalysts, it is clear that the variations are rather large. At the end of each calorimetric experiment, the obtained curve of ($T_r - T_j$) vs. time is transformed into a reac-
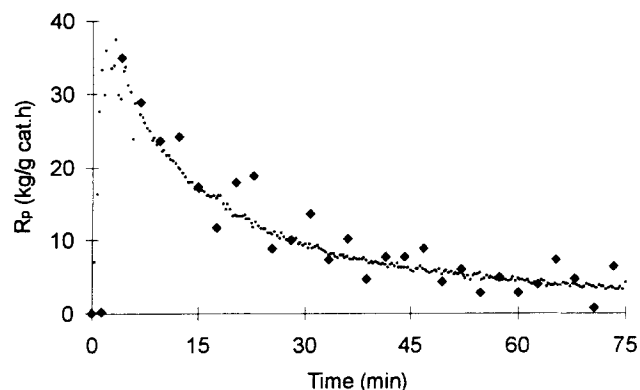

Figure 9. Reaction rate as a function of the time based on GC measurements (♦) and temperature difference over the reactor and the reactor jacket (•).

tion-rate curve by fitting the calculated yield to the weighed yield. The obtained smooth curve is in agreement with the GC-based data and based on eight times more data points and is therefore much more accurate. The GC measurements have been discontinued, and in the more recent experimental program we determined the reaction rate as a function of time from the mentioned temperature difference.

Reproducibility

The reproducibility of the experiments has been tested by repeating a standard experiment at 57°C. This was carried out with 3% hydrogen in the gas cap, a fixed ratio of the concentrations of catalyst, cocatalyst, and electron donor, and a reaction time of 75 min. The results of the repeated experiments are given in Table 3, where the given yield is related to the mass of MgCl$_2$/TiCl$_4$/EB catalyst injected into the reactor. An average yield of 22.4 kg/g catalyst obtained has a maximum deviation of 7%, which is acceptable. To test for catalyst losses during the injection procedure, the standard amount of catalyst has been increased 2.5 times in the last experiment of the series. Because the yield, obtained in this experiment with a high catalyst dosage, has been found to be 1.9% *below* the average yield, catalyst losses can be assumed to be negligible. Throughout the later experimental program, the standard experiment has been executed regularly to check the monomer purity, the catalyst stability, and the condition of the experiment.

Table 2. Flory–Huggins Interaction Parameter χ and the Volume Fraction of Monomer in Polymer ϕ at Liquid Pool Conditions

T (°C)	χ	ϕ
27	0.76	0.51
37	0.83	0.44
47	0.92	0.37
57	1.05	0.29
67	1.26	0.21

Table 3. Yields from Repeated, Standard Experiment at 57°C with a Fixed Ratio of 500 mol/mol Al/Ti and 2 mol/mol Al/PEEB, 3% H$_2$ in the Gas Cap and a Reaction Time of 75 min

Exp. No.	Catalyst (mg)	Yield (kg/g Cat)	Dev. from Avg. (%)
1	15.9	23.9	+ 6.6
2	16.0	22.7	+ 1.2
3	15.8	22.2	− 1.0
4	16.3	21.1	− 5.9
5	15.6	23.5	+ 4.8
6	16.6	21.6	− 3.7
7	40.2	22.0	− 1.9

Table 4. Yields from Repeated Experiment at Different Temperatures with a Fixed Ratio of 115 Al/Ti and 2 mol/mol Al/PEEB and a Hydrogen Concentration of 3% in the Gas Cap

Exp. No.	T (°C)	Catalyst (mg)	Yield (kg/g Cat)	Dev. from Avg. (%)
1	27	100	3.7	−3.5
2	27	139	3.9	+1.8
3	27	139	3.9	+1.8
4	37	72	8.4	+2.4
5	37	70	8.0	−2.4
6	47	48	14.3	+1.4
7	47	36	13.9	−1.4
8	57	20	18.3	−1.3
9	57	28	18.8	+1.3

Figure 10. Polymer yield/g MgCl$_2$/TiCl$_4$/EB catalyst after 75-min reaction as a function of temperature.

Reproducibility was also tested at different temperatures (Table 4). The table shows that the yield per gram catalyst of duplicates is always of the same order and independent of catalyst charge. This again supports our conclusion that catalyst losses are within the total error.

The first stage of the polymerization has not been considered in this study, but see Kim et al. (1994).

The influence of temperature

In the next series of experiments, the temperature was varied from 27°C to 67°C with a constant ratio of the catalyst, cocatalyst, and electron donor. Based on these experiments we studied the decay behavior of the catalyst and estimated the initial reaction rates, that is, the initial reaction rate for instantaneously activated catalyst. Table 5 gives an overall summary of the experiments, presenting the reaction conditions, conversions, yields, induction time, and the initial and maximum reaction rates at different temperatures. Further, it gives the fitted deactivation constants and the relative error of the simulations. Below, a general description is given of the experimental results and after that the determination of the various kinetic parameters explained in detail.

Figure 10 shows the yield per gram MgCl$_2$/TiCl$_4$/EB catalyst obtained at different temperatures for a reaction time of
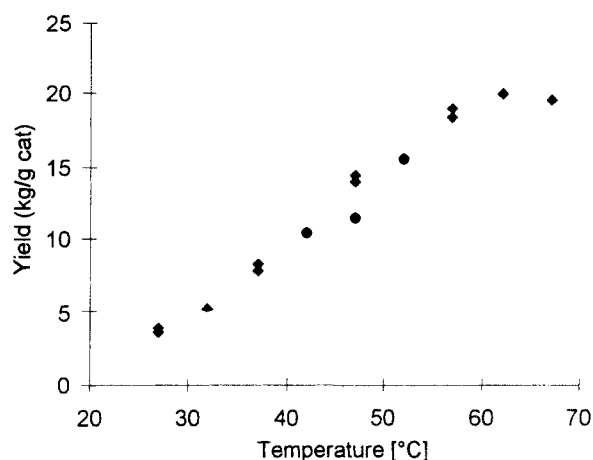
75 min. The yield increases with temperature and becomes constant at temperatures above 65°C, which is in agreement with earlier results for MgCl$_2$-supported catalysts (Doi et al., 1982). Figure 11 shows the reaction rate as a function of time at temperatures ranging from 27°C to 67°C: the reaction-rate curves are strongly influenced by temperature, both at the maximum rate as well as at the decay rate. The initial catalyst activity approximately doubles with every 10°C increase in temperature, and even exceeds an activity of 100 kg/g cat·h at 67°C. In addition, the deactivation rate of the catalyst also increases rapidly with temperature. At 67°C the catalyst decays so fast that after a 15-min reaction time, the polymerization rate is even lower than the rate at 57°C. Various explanations are given in the literature for this extremely fast decay at higher temperatures of the catalyst in the first stage of the reaction, for example, chemical deactivation, thermal runaway in the particles, and diffusion limitations. Interpreting their experiments, many authors have rejected the possible diffusion limitation of monomer through the polymer, encapsulating the active centers, as a likely explanation for the

Table 5. Experiments: Reaction Conditions, Conversion, Yield, Induction Time, Initial and Maximum Reaction Rates, Deactivation Constants and the Error of Simulations*

Run	T (°C)	Cat. (mg)	H$_2$ (vol. %)	C_m in Poly. (kg/m^3)	ζ	Yield (kg/g Cat)	t_i (min)	$R_{p,max}$ (kg/g Cat·h)	$R_{p,0}$ (kg/g Cat·h)	K_D g Cat/m^3
1	27	138.8	3.4	300	0.40	3.9	3.0	9.1	9.7	121
2	27	100.1	4.0	300	0.27	3.7	2.0	7.1	7.3	110
3	27	139.7	3.8	300	0.41	3.9	2.0	7.0	7.2	102
4	32	103.8	4.1	295	0.41	5.3	2.3	10.6	11.0	84
5	37	70.1	3.8	289	0.37	8.0	2.3	17.2	18.0	60
6	37	72.0	3.7	289	0.41	8.3	2.3	19.5	20.4	58
7	42	53.4	4.0	283	0.42	10.5	3.7	25.3	27.8	53
8	47	35.7	3.3	277	0.45	13.9	2.3	34.9	37.1	40
9	47	36.2	3.6	277	0.51	11.3	2.3	40.9	44.1	42
10	47	47.7	3.5	277	0.31	14.3	2.3	33.3	35.0	35
11	52	32.1	3.3	270	0.37	15.5	1.7	46.5	49.6	42
12	57	28.2	3.3	263	0.27	18.8	2.7	52.8	57.8	32
13	57	19.7	2.9	263	0.26	18.3	3.3	45.7	50.3	31
14	62	26.8	3.2	256	0.40	19.9	2.0	102.2	118.0	35
15	67	25.5	3.4	247	0.37	19.4	1.7	116.2	134.4	36
16	67	25.8	3.1	247	0.37	19.4	1.7	101.7	115.7	36

*The presented kinetic parameters are based on a deactivation order of 2.0.
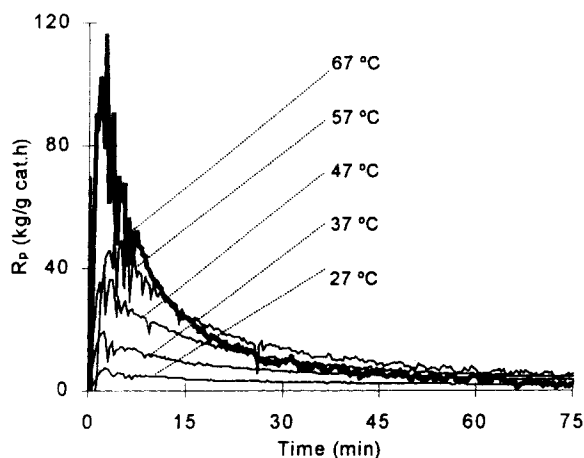
Figure 11. Typical reaction rates at 27–67°C with a reaction time of 75 min.

Figure 12. Order of deactivation as a function of temperature for simulation of the experimental data with an optimized set of n, K_D, and $R_{p,0}$.

strong decay measured with $MgCl_2/TiCl_4$ catalysts. Deactivation of these catalysts is believed to be a more likely result of the deactivation of the propagation centers during the reaction. The most likely explanation for this deactivation is *chemical* deactivation, for example, through the reduction of active Ti^{3+} to nonactive Ti^{2+} and the poisoning of active centers by the reaction products of reactions between the various catalyst components. At higher temperatures, thermal deactivation due to temperature runaway in the particles and, as recently suggested by Han-Adebekun et al. (1997), diffusion limitation due to partial polymer melting may also play a role in the deactivation of the catalyst.

Determination of kinetic parameters

The kinetic parameters n, K_D, and $R_{p,0}$ have been determined by fitting the experimental reaction-rate curves to Eq. 15, the kinetic model described earlier in this article. Because the model does not take into account the activation process during the induction period, this fitting is based on the reaction-rate data after that period up to the end of the reaction at 75 min. The induction period has been considered to be the time up to the maximum reaction rate, typically 2 to 5 min.

Determination of the Deactivation Order, n. The value of the deactivation order, n, is a recurrent point of discussion (Barbè et al., 1987; Brockmeier and Rogan, 1985; Doi et al., 1982). According to Barbè, the experimental kinetics curves cannot be fitted to a single model for deactivation of the first or second order because the decay behavior may be influenced by many factors, such as catalyst type, reaction time, process type, and a plurality of site types.

To determine the deactivation order of our catalyst system, the experimental-rate curves have been fitted with an optimized set of the kinetic parameters n, $R_{p,0}$, and K_D. Multiplicity in the optimization procedure is avoided by using $R_{p,\max}$ as the initial value and restricting n to values between one and three. Figure 12 shows that the optimized order of deactivation decreases from three to one with increasing temperature. An explanation for this change may be found in the existence of various mechanisms of deactivation that depend
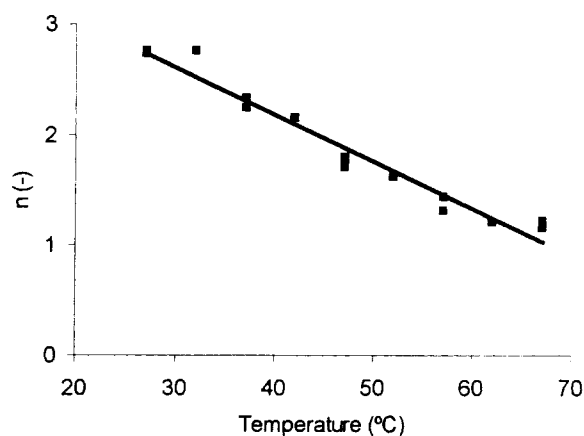
in a different way on temperature. We tested the model using an average, fixed deactivation order over the entire temperature range. To choose the appropriate deactivation order, the experimental curves have been fitted with $n = 1.0$, 1.5, 2.0, and 2.5, successively. Figure 13 shows the relative error as a function of temperature for the better fitting deactivation orders 1.5 and 2.0. In both cases, the error reaches a minimum of about 5% at temperatures of 40 to 50°C and increases to a maximum of about 30% at the lower and higher temperatures. When deactivation orders below 1.5 or above 2.0 are used, relative errors up to 60% are obtained. In our further calculations, we have chosen $n = 2$ because it fits the experimental data relatively well over the entire temperature range.

Determination of the Activation Energy, $E_{a,p}$. The activation energy of the propagation reaction is derived from the estimated initial reaction rates at different temperatures. According to Eq. 15, the initial reaction rate $R_{p,0}$ of an instantaneously activated catalyst is described by the relation:

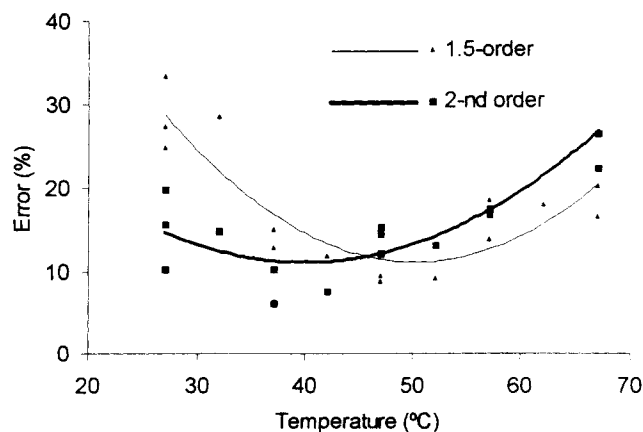$$R_{p,0} = k_p \cdot C_0^* \cdot C_m. \tag{26}$$

Figure 13. Deviation of simulated from the experimental curves as a function of time with fixed deactivation orders of 1.5 and 2.0.
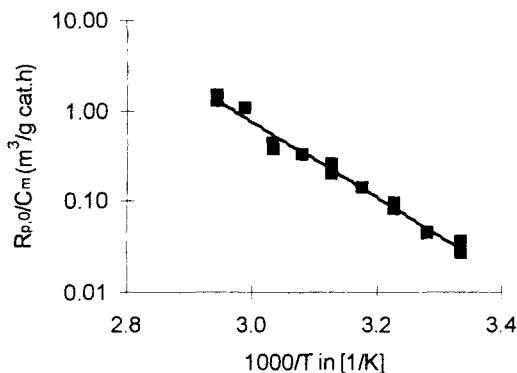
Figure 14. $R_{p,0}/C_m$ **plotted vs. the reciprocal temperature.**

The activation energy of propagation reactions $E_{a,p}$ and kinetic constant $k_{p,0} \cdot C_0^*$ are determined from the slope and intercept, respectively.

By linearization of Eq. 15 or 16, $R_{p,0}$ is easy to determine. In Figure 14, the initial reaction rates calculated are plotted against the reciprocal temperature on the basis of a deactivation order of 2.0. From the data in this figure, the activation energy of the propagation reaction has been estimated to be 79.9 kJ/mol.

Determination of the Deactivation Constant, K_D. The deactivation constant has been determined by fitting the kinetic model, Eq. 15, to the experimental curves after the induction period, using a fixed deactivation order of 2.0. Figure 15 shows that the deactivation constant K_D decreases with increasing temperature. From the data in Figure 15, the activation energy of the deactivation reactions has been estimated to be 35.7 kJ/mol.

The kinetic expression and the associated kinetic parameters are summarized in Eq. 27 and Table 6, respectively:

$$R_p = \left\{ \left(k_{p,0} \cdot C_0^* \cdot C_m \cdot e^{-E_{a,p}/RT} \right)^{(1-n)} \right.$$

$$\left. + (n-1) \cdot \frac{k_d}{k_{p,0}^{n-1}} \cdot e^{[(n-1)E_{a,p} - E_{a,d}]/RT} \cdot (C_m)^{1-n} \cdot t \right\}^{(1/(1-n))}.$$
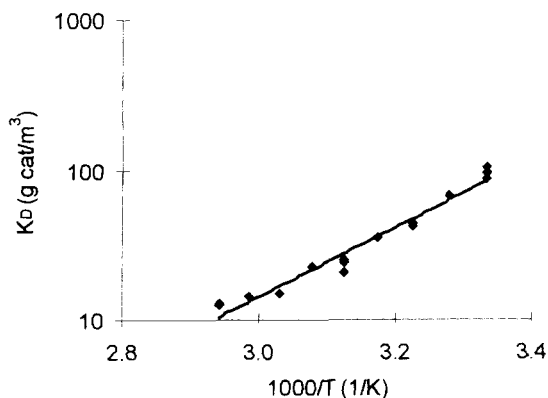
(27)

Figure 15. **Deactivation constant** (K_D) **vs. the reciprocal temperature.**

The activation energy of deactivation reactions $E_{a,d}$ and kinetic constant $k_d/k_{p,0}$ are determined from the slope and intercept, respectively.

Table 6. Parameters Belonging to the Kinetic Model in Eq. 27

n	$E_{a,p}$ (kJ/mol)	$E_{a,d}$ (kJ/mol)	$k_{p,0} \cdot C_0^*$ (m³/g cat)	$k_d/k_{p,0}$ (m³·g cat/h)	Validity Range
2	79.9	35.7	2.4×10^{12}	$1.7^* \times 10^{-6}$	27–67°C

Figures 16a and 16b show the experimental and the simulated curves at a temperature of 42 and 67°C, respectively, and give an indication of the accuracy of the kinetic model. At 42°C the experimental curve is described within an error of 7%; at 67°C the error is the largest, 22%, because the deactivation order of 2.0 fits the curves less well at higher temperatures. Nevertheless, the result is not too bad, considering the complex nature of the kinetics.

The influence of prepolymerization

The influence of the prepolymerization on the reaction-rate curves has been studied by starting the reaction in cold liquid propylene. After a few minutes, the reactor temperature is quickly raised to execute the polymerization at the desired
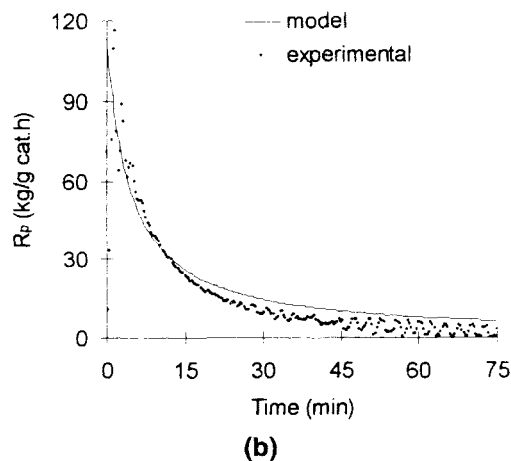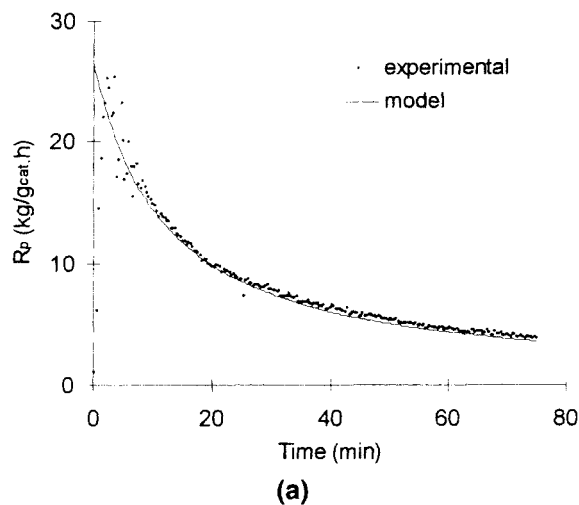

(a)

(b)

Figure 16. **Experimental and simulated reaction rates of an experiment: (a) at 42°C; (b) at 67°C.**

Table 7. Polymerizations at 57, 67 and 72°C With and Without a Prepolymerization Step in Liquid Propylene at Below the Reaction Temperature

Exp. No.	Prepoly. Step	$T_{reaction}$ (°C)	$T_{prepoly}$ (°C)	$t_{prepoly}$ (min)	Yield (kg/g Cat)
1	No	57	—	—	18.3
2	Yes	57	23	6	21.0
3	Yes	57	42	1	20.3
4	No	67	—	—	19.4
5	Yes	67	27	1	22.2
6	Yes	67	27	1	23.4
7	Yes	67	42	1	23.3
8	Yes	67	47	1	22.7
9	Yes	67	47	10	24.5
10	Yes	72	72	1	17.4

reaction temperature during the remaining reaction time. We have investigated polymerizations at 57°C, 67°C, and 72°C, using prepolymerization temperatures of 23 to 47°C and prepolymerization times of one to 10 minutes (see Table 7). This table shows prepolymerization increases the yield by 20 to 30%.

Figure 17a shows the reaction-rate curves of three experiments executed at 57°C; one experiment without prepolymerization and two experiments with prepolymerization at 23 and 42°C, respectively. After prepolymerization the reaction rates are significantly higher than without prepolymerization. The high reaction rate after prepolymerization at 23°C is remarkable. Note that the reaction-rate curves coincide after a reaction time of 30 to 40 min. Figure 17b shows that for three similar experiments, now at 67°C, the experiment with the lowest prepolymerization temperature again gives the highest yield and reaction rates. Figure 17c shows that for three similar experiments at 67°C and prepolymerization at 47°C for 1 min and 10 min, respectively, we have a remarkably high yield for the prepolymerization time of 10 min. The high yield is a result of a relatively high reaction rate during the prepolymerization at 47°C, followed by relatively slow decay *after* the prepolymerization.

Figure 18 shows the reaction-rate curves of two experiments at 67°C and one experiment at 72°C, with and without prepolymerization. The experiment executed at 72°C with a prepolymerization at 42°C shows a very high peak activity, reached after about 6 min. The peak is followed immediately by strong decay, resulting in a completely deactivated catalyst after 40 min and a relatively low polymer yield.

There are several explanations for the observed increase in reaction rate and yield for experiments with a prepolymerization step. In the first place, the activation process of potentially active centers may be more efficient at low temperatures. Since the polymerization rate is much lower, there is more chance for the cocatalyst to diffuse inside the primary catalyst particle to form active centers at the potentially active Ti-sites. Furthermore, the primary catalyst particles are protected against a thermal runaway at low temperatures, as the reaction heat production rate is much lower at the low prepolymerization temperatures. The particles have time to grow in a controlled way to a size where the external particle surface area is large enough to remove all the heat of reaction produced and to maintain the particle at the required polymerization temperatures.
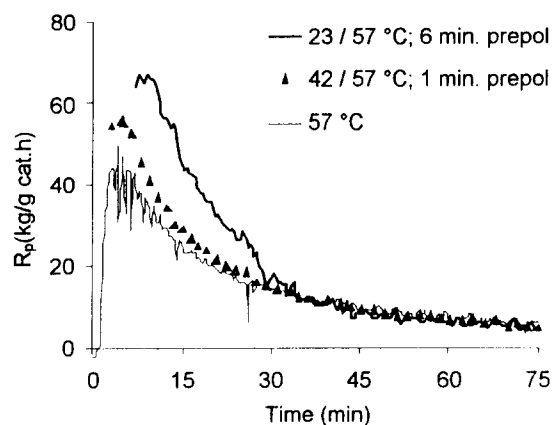
(a)
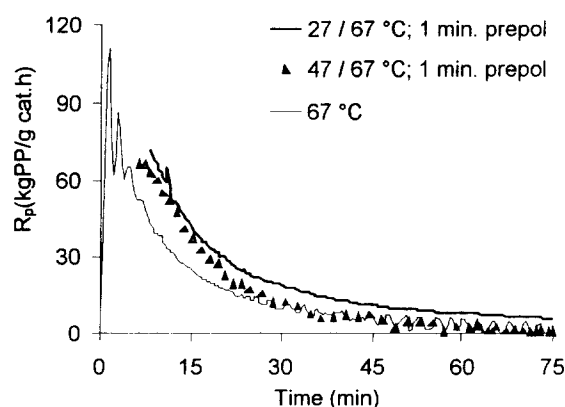
(b)
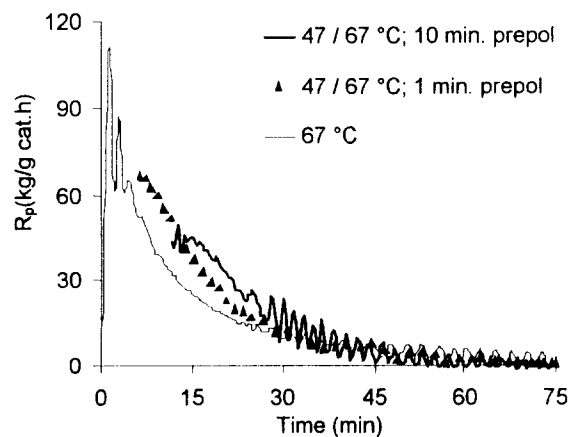
(c)

Figure 17. Reaction rates of polymerizations without and with prepolymerization: (a) $T_r = 57$°C, $t_{prepoly} = 1$ min, $T_{prepoly} = 23$ and 47°C; (b) $T_r = 67$°C, $t_{prepoly} = 1$ and 6 min, and $T_{prepoly} = 23$ and 47°C, respectively; (c) $T_r = 57$°C, $t_{prepoly} = 1$ and 10 min, and $T_{prepoly} = 47$°C.

Conclusions

An experimental setup for the polymerization of propylene in liquid monomer has been presented comprising a jacketed 5-L reactor, a liquid propylene purification system, a catalyst
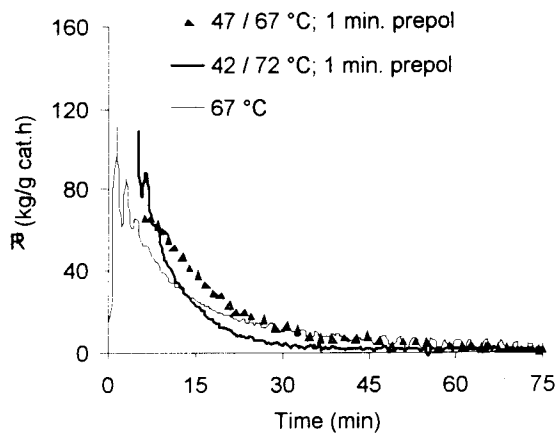
Figure 18. Reaction rate of polymerizations at 67°C without and with prepolymerization during 1 min, and the reaction-rate curve of a polymerization at 72°C with prepolymerization at 42°C during 1 min.

injection system, and a temperature control system. Reaction rates have been measured accurately as a function of time on the basis of the temperature difference between the reactor and the jacket of the reactor. The experiments have proven to be reproducible within 7%. The reaction-rate curves also have been determined on the basis of concentration measurements by GC, but considerably less accurately.

A series of experiments has been executed in the temperature range of 27 to 67°C with a hydrogen concentration of about 3% in the gas cap and a fixed ratio of catalyst components. The experimentally measured reaction-rate curves have been simulated with a model containing three parameters: the order of deactivation, n, the deactivation constant, K_D, and the initial reaction rate, $R_{p,0}$. Simulations of the experimental-rate curves with such a model has shown that the optimized order of deactivation is between one and three, and decreases with increasing temperature. However, as K_D and n are mutually dependent, it is necessary to set the deactivation order in the kinetic model to a fixed value. We have set the deactivation order at 2.0 because it fits the experimental curves acceptable over the entire temperature range. From the calculated initial reaction rates and the estimated concentration of monomer in the polymer, the activation energy of the lumped propagation reactions has been estimated to be 79.9 kJ/mol. The activation energy of the deactivation reactions has been estimated to be 35.7 kJ/mol. The proposed kinetic model is valid for a broad temperature range and describes the experimental curves mostly within an error of 15%, and at a maximum error of 25%.

Prepolymerization of the catalyst in cold, liquid propylene for a few minutes has a strong influence on the reaction rate and decay behavior later on. Without exception, prepolymerization increases the final polymer yield by 20 to 30% compared to reactions without prepolymerization. The increase in yield is a particular result of the relatively high reaction rates obtained during the first 30 to 40 min of reaction time *after* the prepolymerization. Further, the highest yields have been obtained in experiments with the lowest prepolymerization temperatures.

Concluding that prepolymerization does increase the reaction rate and the yield of a polymerization reaction significantly can summarize the results of the prepolymerization experiments. For a given catalyst, the required conditions of prepolymerization depend on the desired final polymerization temperature. Experiments executed at high temperatures require a longer prepolymerization at milder conditions.

Although the study in this article gives us a kinetic model and its constants for the polymerization of propylene in liquid monomer with a rapidly deactivating Ziegler–Natta catalyst, one should be careful in applying the results, as kinetics can vary strongly from catalyst to catalyst. Moreover, changes in the concentration of hydrogen or changes in the ratios between catalyst, cocatalyst, and electron donor can also have a strong influence on the reaction rates.

In our more recent work (Samson et al., 1998a,b), we investigate the influence of the concentrations of hydrogen, catalyst, cocatalyst, and electron donor on the polymerization kinetics. Moreover, we investigate the kinetics of the gas-phase polymerization with exactly the same catalyst system and compared them with the kinetics in liquid propylene as presented in this article (Samson et al., 1998).

Notation

R = gas constant, J/mol·K
R_p = polymerization rate, kg/g cat·s
R_0 = initial polymerization rate, kg/g cat·s
T_c = critical temperature, K
T_r = reactor temperature, K
V_m = volume fraction of polymer
w = weight fraction
η = viscosity, kg·m^{-1}·s^{-1}
λ = conductivity, W·m^{-1}·K^{-1}
ρ = density, kg·m^{-3}
ζ = conversion

Subscripts

exp = experimental
cat = catalyst
  i = induction period
  p = polymerization
PP = polypropylene
sim = simulation, simulated

Literature Cited

Aminabhavi, T. M., H. T. S. Phayde, and J. D. Ortego, "A Study of Sorption/Desorption and Diffusion of *n*-Alkanes and Aliphatic Hydrocarbons into Polymeric Blends of Ethylene-Propylene Random Co-Polymer and Isotactic Polypropylene in the Temperature Interval of 25 to 70°C," *J. Poly. Eng.*, **16**, 121 (1996).

Barton, A. F. M., *CRC Handbook of Polymer-Liquid Interaction Parameters and Solubility Parameters*, CRC Press, Boca Raton, FL, p. 284 (1990).

Böhm, L. L., "Reaction Rate Model for Ziegler-Natta Polymerization Processes," *Polymer*, **19**, 545 (1978).

Bradford, M. L., and G. Thodos, "Solubility Parameters of Hydrocarbons," *Can. J. Chem. Eng.*, **44**, 345 (1966).

Brockmeier, N. F., and J. B. Rogan, "Propylene Polymerization Kinetics in a Semi-Batch Reactor by Use of a Supported Catalyst," *Ind. Eng. Chem. Prod. Res. Dev.*, **24**, 278 (1985).

Doi, Y., T. Keii, E. Suzuki, and M. Tamura, "Propene Polymerization with a Magnesium Chloride Supported Ziegler Catalyst 1," *Macromol. Chem.*, **183**, 2285 (1982).

Gunn, D. J., "Transfer of Heat or Mass to Particles in Fixed and Fluidised Beds," *Int. J. Heat Mass Transfer*, **21**, 467 (1978).

Han-Adebekun, G. C., M. Hamba, and W. H. Ray, "Kinetic Study of Gas Phase Olefin Polymerization with a $TiCl_4/MgCl_2$ Catalyst I. Effect of Polymerization Conditions," *J. Poly. Sci. Part A Poly. Chem.*, **35**, 2063 (1997).

Hutchinson, R. A., and W. H. Ray, "Polymerization of Olefins through Heterogeneous Catalysis," *J. Appl. Polym. Sci.*, **41**, 51 (1990).

Kim, I., and S. I. Woo, "Polymerization of Propylene by Highly Active Catalysts Synthesized with $Mg(OEt)_2$/Benzoyl Chloride/$TiCl_4$," *Poly. Bull.*, **23**, 35 (1990).

Kim, J. H., I. Kim, and S. I. Woo, "Computer Simulation Study of Ethylene Polymerization Rate Profile Catalyzed Over Highly Active Ziegler-Natta Catalysts," *Ind. Eng. Chem. Res.*, **30**, 2074 (1991).

Kim, I., H. K. Choi, J. H. Kim, and S. I. Woo, "Kinetics of Propylene Polymerization in the Initial Acceleration Stage," *J. Poly. Sci. Part A Poly. Chem.*, **32**, 971 (1994).

Perry, R. J., "Introducing Catalyst into a Reactor," U.S. Patent No. 3,780,135 (1973).

Samson, J. J. C., G. Weickert, and K. R. Westerterp, "Gas Phase Polymerization of Propylene with a Highly Active Catalyst," *submitted* (1998a).

Samson, J. J. C., P. J. Bosman, G. Weickert, and K. R. Westerterp, "Liquid Phase Polymerization of Propylene with a Highly Active $MgCl_2/TiCl_4$/EB Catalyst: The Influence of Hydrogen, Cocatalyst and Electron Donor on Reaction Kinetics," in press (1998b).

Tait, P. T. J., D. R. Burfield, and I. D. McKenzie, "Ziegler-Natta Catalysis: 1. A General Kinetic Scheme," *Polymer*, **13**, 302 (1972).

Yuan, H. G., and W. H. Ray, "Polymerization of Olefins through Heterogeneous Catalysis 1," *J. Appl. Poly. Sci.*, **27**, 1691 (1982).

Zakharov, V. A., G. D. Bukatov, and Y. I. Yermakov, "On the Mechanism of Olefin Polymerization by Ziegler-Natta Catalysts," *Adv. Poly. Sci.*, **51**, 61 (1983).